Maxwell Stress Induced Flow-Deformation and Optical Nonlinearities in Liquid Crystals

Iam C. Khoo*, **Shuo Zhao, Chun-Wei Chen, and Tsung-Jui Ho**

(*Invited Paper*)

Abstract—We present a critical account of intense pulsed-laser field induced refractive index changes caused by flow, crystalline axis reorientation and distortion and other high order photonic processes in transparent liquid crystals. In particular, the optical nonlinearity associated with Maxwell Stress induced flow-reorientation in nematic liquid crystals is explicitly calculated, and their possibility for all-optical switching application is experimentally demonstrated. Similar flows processes have also been observed in Blue-Phase liquid crystals with nanosecond and picosecond pulsed-lasers.

1. INTRODUCTION

Maxwell equations and the constitutive equations for the material response [1] are ubiquitous in all fundamental and applied studies of *optical material and device physics.* Perhaps the most frequently studied material response is the polarizations $\mathbf{P}(\mathbf{r};t)$ induced by an optical electric field $\mathbf{E}(\mathbf{r};t)$. In general, one could separate $\mathbf{P}$ into a linear and a nonlinear term of the form [2–4]:

$$\mathbf{P}_L = \varepsilon_o \chi^{(1)} : \mathbf{E}$$
$$\mathbf{P}_{\mathrm{NL}} = \varepsilon_o \boldsymbol{\chi}^{(2)} : \mathbf{EE} + \varepsilon_o \boldsymbol{\chi}^{(3)} : \mathbf{EEE} + \ldots$$

Here $\boldsymbol{\chi}^{(1)}$, $\boldsymbol{\chi}^{(2)}$, $\boldsymbol{\chi}^{(3)}$ are the respective linear, second and third order susceptibility tensors characterizing the response of the medium to the electric field. The linear term $\mathbf{P}_L$ gives rise to the complex refractive index that describes various dispersion, modes and propagation characteristics, whereas $\mathbf{P}_{\mathrm{NL}}$ contains higher-order dependence on the electric field. In centro symmetric materials such as liquid crystals [2], the first non-vanishing term is the 3rd order nonlinear polarization term $\mathbf{P}^{(3)} = \varepsilon_o \chi^{(3)} : \mathbf{EEE}$. In general, since the material possesses a multitude of resonance frequencies ω_i's, while the incident electric field could carry many temporal and spatial frequency components k and ω's, the third order polarization $\mathbf{P}^{(3)}$ gives rise to a rich variety of phenomena due to wave mixing processes.

Among the various nonlinear optical wave mixing processes possible with $\mathbf{P}^{(3)}$ are those arising from a term of the form $\mathbf{P}^{(3)} = \varepsilon_o \chi^{(3)} |E|^2 \mathbf{E}(\omega)$. In analogy to the first order linear term, this is equivalent to having an electric field induced dielectric constant change $\Delta \varepsilon = \varepsilon_o \chi^{(3)} |E|^2$ or equivalently a refractive index change $\Delta n \sim |E|^2$. In nonlinear optical studies, the refractive index change is usually expressed in the form $\Delta n = n_2 I$, where $I[I = (1/2\eta)|E|^2$ with η the impedance] is the intensity of the laser and n_2 is the Kerr constant but is more often called the nonlinear index coefficient or optical nonlinearity. It is important to note here that what is conventionally known as electro-optics where an applied low frequency electric field is used to produce index change in a material so as to modulate its optical properties also falls under this category of third order nonlinearity.

Liquid crystals are arguably the most nonlinear and electro-optics active materials owing to their unique physical properties and extreme sensitivities to external fields [2–6]. Generally we can classify the mechanisms for index change in liquid crystals into two distinct types: (i) those originating from individual molecules, and (ii) collective crystalline responses. Individual molecular electronic responses of liquid crystals are similar to other organic materials, and come from single- and multi-photonic transitions amongst the molecular energy levels [4, 7–12]. These responses are ultrafast [sub-ps to fs] and generally the non-resonant nonlinear index coefficients are in the range of 10^{-14}–10^{-12} cm^2/Watt; they have been exploited for ultrafast nonlinear optics such as stimulated scatterings, third harmonic generations, multiphoton absorptions, femtosecond laser pulse compression studies...etc.

Collective responses of liquid crystals such as crystalline axis rotation, order parameter modifications and thermal/density changes, flows and macroscopic material movement [2–6; 13–23] are characterized by much larger nonlinear index coefficients that could range over 13 decades from $\sim 10^{-10}$ to 10^3 cm^2/Watt, and slower response times on the order of 10's nanoseconds to milliseconds and longer. As a result of such nonlinearity and extreme sensitivities to external field, NLC have been a favorite material for incorporation in specialized micro- and nano-structure for tunable optical devices or switches [23–32] with low power threshold requirement. In this article, we will delve into a hitherto relatively unexplored physical property that is *unique to transparent liquid crystals*, namely, the ability to flow and a strong coupling between *flow and crystalline axis rotation or lattice distortion* under the action of an applied field. Specifically, we will focus on the so-called *Maxwell Stress* [1, 14] exerted by the electric field of an intense pulsed laser. We shall illustrate such nonlinear optical processes with two examples: (i) flow-reorientation in nematic liquid crystals (NLC) and (ii) flow induced lattice distortion in Blue-Phase liquid crystal (BPLC).

2. MAXWELL STRESS INDUCED FLOW-REORIENTATION NONLINEARITY IN NEMATIC LIQUID CRYSTALS

Maxwell Stress was first invoked by Eichler and Macdonald [14] to interpret flow-reorientation effect produced by an optical polarization grating in an aligned nematic liquid crystal. Figure 1 depicts schematically the experimental set-up. The liquid crystal is homeotropically aligned in the z-direction. Two obliquely-incident (at an angle β) coherent laser beams [derived from splitting a pump laser beam] with equal intensity and perpendicular polarizations intersect at a small wave mixing angle on the NLC, i.e., the optical electric field vector is given by $[E(t)e^{ik_ty+ik_lz}, E(t)e^{-ik_ty+ik_lz}, 0]$ which imparts a *polarization grating on the sample with a grating wave vector* $\mathbf{2k_t}$ along the y-axis.

Since optical frequencies are in the 10^{14} s^{-1} region, the Maxwell Stress at work here is the time-
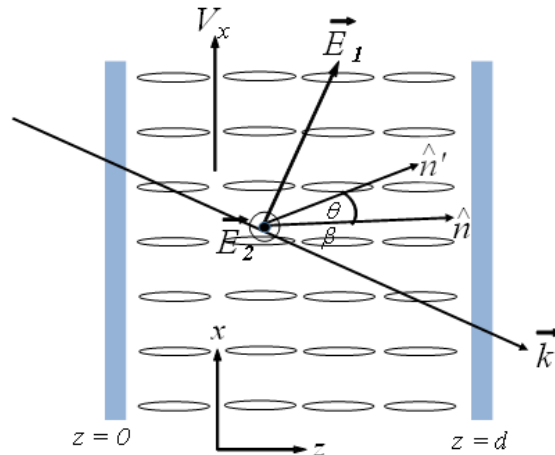

Figure 1. Side view of coherent optical wave mixing of two crossed-polarized lasers in a homeotropically aligned NLC cell.

averaged force given by:

$$\langle f_E \rangle = \frac{1}{2} \text{Re} \left[(\nabla \cdot D) E^* - D \times \nabla \times E^* \right] \tag{1}$$

Under the action of the optical fields given above, it can be shown that we have the following components:

$$\langle f_{E,x} \rangle = -\frac{1}{2} \varepsilon_0 \varepsilon_\perp q_t E_0^2(t) \sin(q_t y) \left(\langle f_{E,y} \rangle = 0, \langle f_{E,z} \rangle = 0 \right) \tag{2}$$

Here $q_t \equiv 2k_t$ is the magnitude of the grating-vector, with a grating constant $\Lambda = 2\pi/q_t$. The general equations describing the coupled flow- reorientation process are of the form [14]:

$$\rho_0 \frac{\partial v_x}{\partial t} - \eta \Delta v_x = F_x \tag{3}$$

$$\gamma_1 \frac{\partial \theta}{\partial t} - K \nabla^2 \theta + \frac{1}{2} \left(\gamma_1 + \gamma_2 \cos 2\theta \right) \frac{\partial v_x}{\partial y} = 0 \tag{4}$$

Here θ is the director axis reorientation angle, v_x the velocity flow (in the x-direction), K the elastic constant; γ_1, γ_2 and η are the viscosity coefficients. F_x in Equation (3) is non-vanishing x-component of $\langle f_E \rangle$ given in (2), which causes flow along the x-direction $[v_x, 0, 0]$. Using (2) and considering only flow in the x-direction, we thus have the following coupled flow-reorientation equations:

$$\rho \frac{\partial v_x}{\partial t} - \eta \frac{\partial^2 v_x}{\partial y^2} = -\frac{1}{2} \varepsilon_0 \varepsilon_\perp q_t \left| E(t) E^*(t) \right| \sin(q_t y). \tag{5}$$

$$\gamma_1 \frac{\partial \varphi}{\partial t} - K \frac{\partial^2 \varphi}{\partial y^2} + \frac{1}{2} \left(\gamma_1 + \gamma_2 \cos 2\varphi \right) \frac{\partial v_x}{\partial y} = 0. \tag{6}$$

2.1. Estimate of Optical Nonlinearity — Flat-Top Square Pulse

We shall estimate the magnitude of the nonlinear index coefficient associated with such laser induced reorientation by considering the case where the two coherent excitation beams are represented by a top-hat function, i.e.,

$$|E(t) E^*(t)| = \begin{cases} E_0^2 & (0 \le t \le \tau_p) \\ 0 & (t < 0, \, t > \tau_p) \end{cases} \tag{7}$$

Ignoring the surface anchoring at the cell boundaries ($z = 0$ and $z = d$), the solutions for the velocity v_x and reorientation angle φ are therefore of the form:

$$v_x = v_m \sin(q_t y); \quad \varphi = \varphi_m \cos(q_t y) \tag{8}$$

From Equation (6), we thus have:

$$\gamma_1 \frac{\partial \varphi_m}{\partial t} \cos(q_t y) + K q_t^2 \varphi_m \cos(q_t y) + \frac{1}{2} \left(\gamma_1 + \gamma_2 \right) q_t v_m \cos(q_t y) = 0 \tag{9}$$

This yields:

$$v_m = -\frac{2}{(\gamma_1 + \gamma_2) q_t} \left[\gamma_1 \frac{\partial \varphi_m}{\partial t} + K q_t^2 \varphi_m \right] \tag{10}$$

Substituting (10) into (5), we have:

$$A \frac{\partial^2 \varphi_m}{\partial t^2} + B \frac{\partial \varphi_m}{\partial t} + C \varphi_m = -\frac{1}{2} \varepsilon_0 \varepsilon_\perp E_0^2 \tag{11}$$

$$A = \frac{2\rho_0 \gamma_1}{(\gamma_1 + \gamma_2) q_t^2}; \quad B = \frac{2 (\rho_0 K + \eta \gamma_1)}{(\gamma_1 + \gamma_2)}; \quad C = \frac{2\eta K q_t^2}{(\gamma_1 + \gamma_2)} \tag{12}$$

The analytical solution to (11) during the laser pulse ($0 < t < \tau_p$) yields:

$$\varphi(t) = -\frac{\varepsilon_0 \varepsilon_\perp E_0^2 (\gamma_1 + \gamma_2)}{4\eta K q_t^2} \left[1 - \frac{\tau_d e^{-t/\tau_d} - \tau_r e^{-t/\tau_r}}{\tau_d - \tau_r} \right] \tag{13}$$

$$\tau_d = \frac{\gamma_1}{K q_t^2}, \quad \tau_r = \frac{\rho_0}{\eta q_t^2} \tag{14}$$

Using the values for the following parameters: $\rho_0 = 10^3 \, \text{kg/m}^3$, $\gamma_1 = 0.01 \, \text{kg/m·s}$, $\eta = 0.02 \, \text{kg/m·s}$, $K = 10^{-12} \, \text{kg·m/s}^2$, and grating period $\Lambda = 20 \, \mu\text{m}$ ($q_t = 2\pi/\Lambda$), the relaxation time $\tau_d \sim 0.1 \, \text{s}$, and the rise time $\tau_r \sim 1 \, \mu\text{s}$. Since $\tau_r \ll \tau_d$, the reorientation angle can be simplified to

$$\varphi_m(t) \approx -\frac{\varepsilon_0 \varepsilon_\perp E_0^2 \, (\gamma_1 + \gamma_2)}{4\eta K q_t^2} \left[1 - \frac{\tau_d e^{-t/\tau_d} - \tau_r e^{-t/\tau_r}}{\tau_d - \tau_r} \right] = \frac{\varepsilon_0 \varepsilon_\perp E_0^2 \, (\gamma_1 + \gamma_2)}{4\eta K q_t^2} \frac{\tau_r}{\tau_d - \tau_r} \left(1 - e^{-t/\tau_r} \right)$$

$$\approx \frac{\varepsilon_0 \varepsilon_\perp E_0^2 \, (\gamma_1 + \gamma_2)}{4\eta K q_t^2} \frac{\tau_r}{\tau_d} \left(1 - e^{-t/\tau_r} \right) \tag{15}$$

Furthermore, in the case where *the laser pulse duration is much shorter than the rise time*, i.e., $\tau_p \ll \tau_r$

$$\varphi_m(t) \approx \frac{\varepsilon_0 \varepsilon_\perp E_0^2 \, (\gamma_1 + \gamma_2)}{4\eta K q_t^2} \frac{\tau_p}{\tau_d} = \varphi_m^{ss} \frac{\tau_p}{\tau_d} \tag{16}$$

As a result of such director axis reorientation, an extraordinary wave (e.g., E_1 in Fig. 1) would experience an index change Δn given by:

$$\Delta n = \frac{n_e(\beta)\varepsilon_a}{n_\perp^2 \cos^2 \beta + n_\parallel^2 \sin^2 \beta} \frac{\sin 2\beta}{2} \cdot \varphi_m = \left(n_2^{SS} \frac{\tau_p}{\tau_d} \right) I \tag{17}$$

$$n_2^{SS} = \frac{\Delta n}{I} = \frac{\varepsilon_\perp \varepsilon_a}{n_e^2(\varphi)} \cdot \frac{(\gamma_1 + \gamma_2) \sin 2\beta}{4c\eta K q_t^2} \tag{18}$$

Here n_2^{SS} is the steady state (for $\tau_p \gg \tau_r$, τ_d) nonlinear index coefficient associated with the laser induced flow-reorientation process. Using the same set of values for the following parameters from: $\gamma_1 = 0.01 \, \text{kg/m·s}$, $\gamma_2 = -1.09\gamma_1$, $\eta = 0.02 \, \text{kg/m·s}$, $K = 10^{-12} \, \text{kg·m/s}^2$, and grating period $\Lambda = 20 \, \mu\text{m}$ ($q_t = 2\pi/\Lambda$), and letting $\sin 2\varphi \sim 1$, n_2^{SS} is estimated to be $\sim 4 \times 10^{-5} \, \text{cm}^2/\text{W}$. Note that if $\tau_p \ll \tau_d$, the effective nonlinear coefficient $n_2^{eff} = n_2^{SS} \frac{\tau_p}{\tau_d}$ is proportionally smaller, just as those effective nonlinearities [2–6] arising from other mechanisms [6] produced by laser pulse that is shorter than the response time.

2.2. Estimate of Optical Nonlinearity — Gaussian Pulse

For the typical case where the input laser pulse is a Gaussian in time, we can solve for the reorientation angle by first obtaining the impulse response of equation for a delta function input driving force, i.e., replace $|E(t)E^*(t)|$ with $E_o^2 \delta(t)$. This yields an *impulse response*:

$$\phi_m = \frac{\varepsilon_0 \varepsilon_\perp E_0^2 \rho_0 \gamma_1}{2q_t^2 \, (\eta\gamma_1 - \rho_0 K)} \left[e^{-t/\tau_d} - e^{-t/\tau_r} \right]. \tag{19}$$

Table 1. Parameters used in flow-orientation simulation.

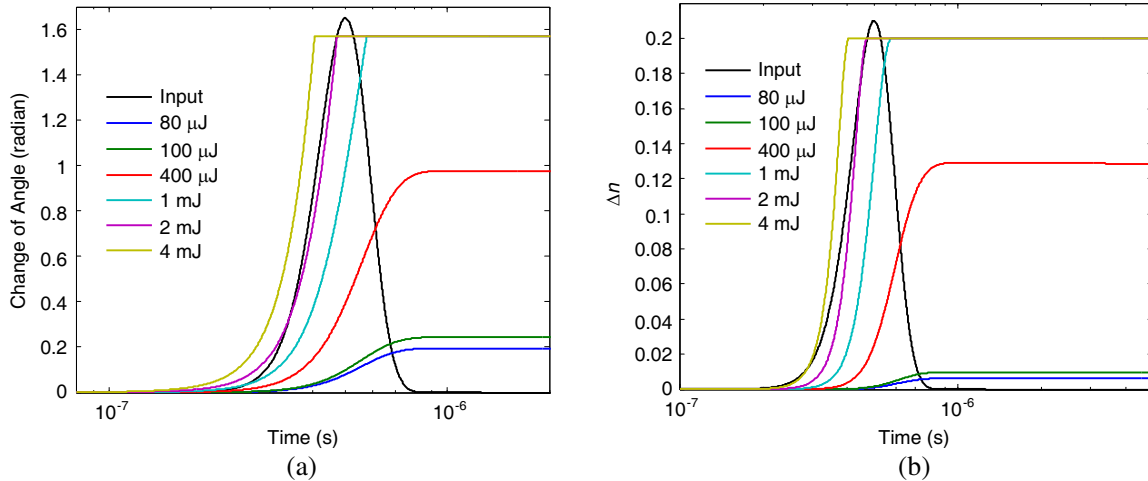| Symbol	Parameter	Value (in SI unit)
ρ_0	Density	$10^3 \, \text{kg/m}^3$
γ_1	Rotational Viscosity	$0.01 \, \text{kg/m·s}$
γ_2	Flow Coupling Rotational Viscosity	$-1.09\gamma_1$
η	Flow Viscosity	$0.02 \, \text{kg/m·s}$
K	Frank Elastic Constant	10^{-12}N
$\varepsilon_\perp/\varepsilon_\parallel$	Ordinary/Extraordinary Dielectric Constant	2.37/3.03
ω_0	Beam Size of Input Laser	$100 \, \mu\text{m}$
τ_p	Pulse duration of Input Laser	$350 \, \text{ns}$

Figure 2. (a) Director axis reorientation angle calculated by convoluting the impulse response with an Gaussian input laser pulse; (b) the corresponding change in extraordinary refractive index. Input laser pulse is included in both figures to ease viewing the time evolution of the calculated parameters.

The *impulse response is then convoluted with the laser pulse*: $E_p(t) = E_0 e^{-(\frac{t-t_0}{\tau_p})^2} e^{i\omega t}$ where τ_p is the pulse duration to give the temporal variation of the reorientation angle $\phi_m(t)$ and the nonlinear index change $\Delta n(t)$.

Using the parameters listed in Table 1, some exemplary simulation results for the time-dependent laser induced reorientation angles and refractive index changes as a function of the input laser energies are shown in Figures 2(a) and 2(b). In general, due to the fact that the relaxation time of director axis reorientation is very long compared to the pulse duration, the reorientation angle and the induced index change are maintained at their peak values for some time long after the pulse is over.

2.3. All-Optical Switching with Twist Alignment Cell

It is imperative to note at this juncture that Equation (19) for the reorientation is derived from an incident laser with a sinusoidal intensity grating profile with a grating constant Λ. In order to make comparison with actual experiments which invariably employ focused laser beams, when analytical or numerical calculation for the complex time dependent multi-dimension propagation is impossible or extremely complicated, one can gain useful insights and obtain reasonable qualitative estimate of the reorientation nonlinearity by replacing the grating factor in (19) by the laser spot diameter, i.e., replacing $1/(q_t)^2 = (\Lambda/2\pi)^2$ by $(2\omega_o)^2$, where $2\omega_o$ is the focused laser spot diameter.
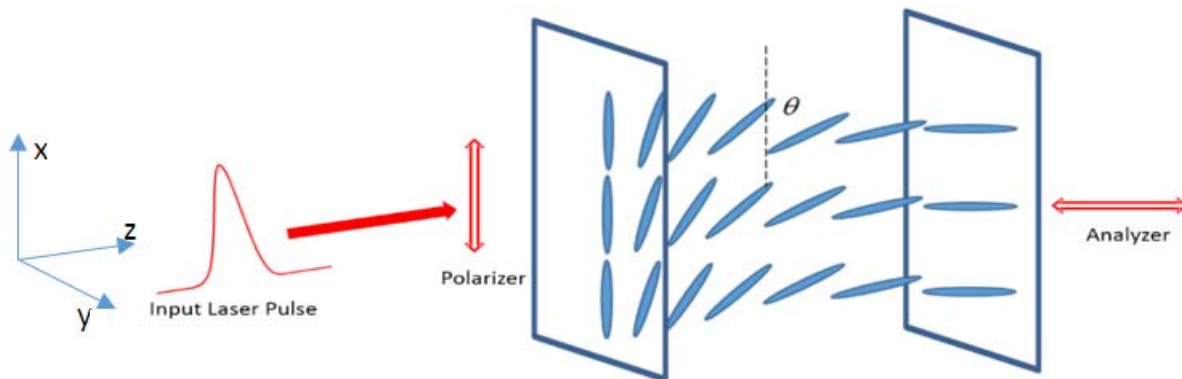

Figure 3. Optical switching cell: Twist nematic liquid crystal sandwiched between crossed polarizers.

The above considerations and approximation allow one to analyze the intensity dependent transmission of a laser pulse through a typical switching set-up involving a 90° twist alignment NLC cell as shown in Figure 3. In conventional electro-optic switches such as those used in LC display panels, the light originating from the back panel is polarized by the input polarizer, with its polarization parallel to the director axis at the input plane. The light intensity being weak, its polarization follows the rotation of the director axis in accordance to Mauguin's theorem, and emerges from the cell with its polarization vector parallel to the output polarizer, i.e., fully transmitted. Switching operation is performed by the AC signal field applied across the NLC cell windows that realigns the director axis to be eventually perpendicular to the cell windows, with the degree of switching-off depending on the field induced reorientation [3].

In electrode-free optical activated transmission switching, the incident light changes or randomizes the director axis orientation by virtue of its intensity [2–6, 29–31]. In the present case, the Maxwell Stress from the *focused* laser beam causes radial flows-reorientation, cf. next section, that randomizes the otherwise well-ordered 90°-twist alignment. This reduces the order parameter and therefore the effective birefringence Δn of NLC from a maximum value of $n_{//} - n_o$ to 0; i.e., the polarization rotation function of the NLC cell is nullified, and the laser that emerges from the NLC cell with the polarization vector orthogonal to the output polarizer will be attenuated. A complete quantitative numerical simulation of the coupled laser induced reorientation, polarization rotation and propagation through the 90°-twist alignment NLC cell is rather complex and is outside the scope of the present discussion. In the following simulations, we have adopted *an approximation* that the birefringence Δn due to such laser induced flow-reorientation process in a 90°-twist alignment sample is represented by $\Delta n = n_2 I(t)$ where n_2 is the effective refractive index coefficient calculated in the preceding section. The birefringence change is then included in the Modified Jones Matrix method [29] to calculate the time dependent transmission using the same set of NLC parameter values listed in Table 1.

Figures 4(a)–(b) show the instantaneous transmittance and the transmitted pulse shape, respectively, for different input laser energies. Below $200\,\mu J$, there is no appreciable change in the transmission throughout the entire pulse; thus the transmitted laser pulse shape is similar to the input. At input laser energies above $200\,\mu J$, the transmission begins to show obvious drop-off at later portion of the pulse. The onset of the transmission switching occurs sooner for higher input laser energies. Such transmission drop-off is reflected in the corresponding transmitted pulse shape in the form of 'switching off' for later portion of the pulse, with the onset of such switching occurring sooner for higher input energies, cf. Figure 4(b). As reported previously [6, 30], these simulations are borne out in experiments studies with sub-microseconds ($\lambda = 750\,nm$) laser pulses. Figures 5(a) and 5(b) show exemplary transmitted laser pulse shapes for two different input laser energies, clearly showing the switching characteristics discussed above. The switching off of the laser pulse occurs earlier for higher input laser energy, similar to the simulated pulse shapes in Figure 4(b).

These switching-offs of the later portion of the laser pulse is reflected in the transmittance defined as the *transmitted laser energy vs. the input*. To simulate the transmittance, the time dependent transmission data used in plotting Figure 4(a) are integrated with the laser pulse shape in time to yield the transmitted laser energy. These results for the intensity dependent transmission are plotted in Figure 6 together with experimental observations for NLC cells of different thicknesses. The experimental results shows that the transmission appears to exhibit an initial switching to a lower (but still high) value at a threshold laser energy of $\sim 10\,\mu J$ (equivalent to a laser peak intensity value $I \sim 1.5 \times 10^5\,W/cm^2$ with a laser spot diameter $2\omega_o \sim 140\,\mu m$). We attribute this to some undetermined mechanism that is highly nonlinear but saturate at low input intensity and therefore does not cause further switching. A more dramatic switching is observed above input laser energy of $200\,\mu J$ corresponding to a peak intensity value $I_{peak} \sim 3 \times 10^6\,W/cm^2$, with an overall dependence on the input energy similar to the simulated result, cf. Figure 6. Despite these qualitative agreements, we need to qualify the findings by noting the fact that several rough approximations have been made in the theoretical simulations for the Maxwell Stress induced flow-reorientation on pulse propagation characteristics as well as in the estimates for various relaxations time constants ...etc. Therefore we do not and cannot expect quantitative agreements. Nevertheless, these theoretical considerations and experimental studies provide one with good insights into the working of Maxwell stress induced flow-reorientation for all-optical switching applications.
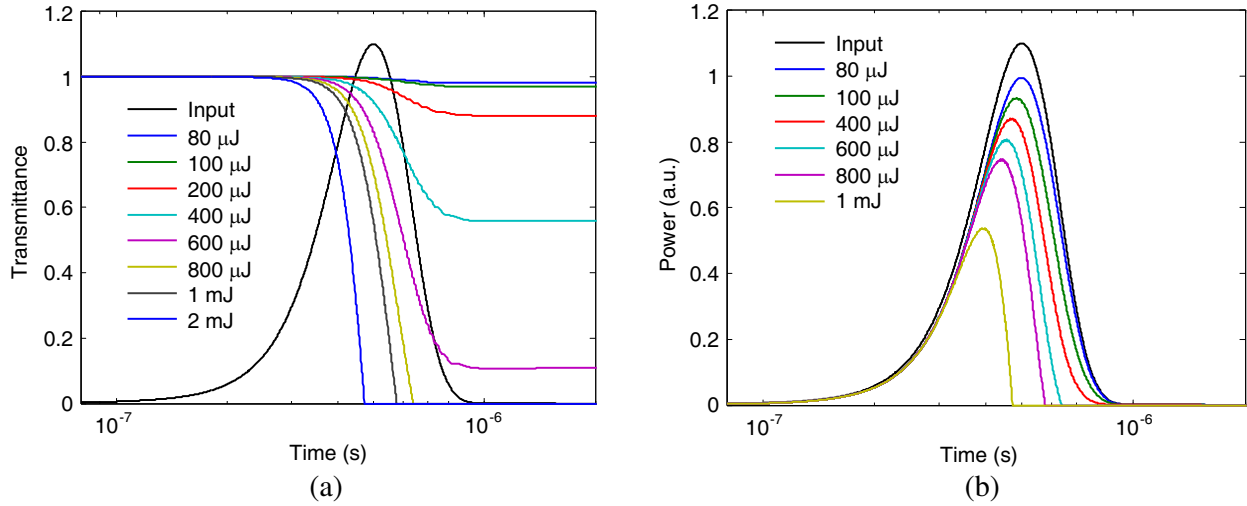
Figure 4. (a) Dynamical evolution of the transmittance change during the laser pulse for different input energies; input pulse shape is also plotted to ease viewing the onset and time evolution of the transmittance. (b) Input V.S. output pulse shapes under different input pulse energies.
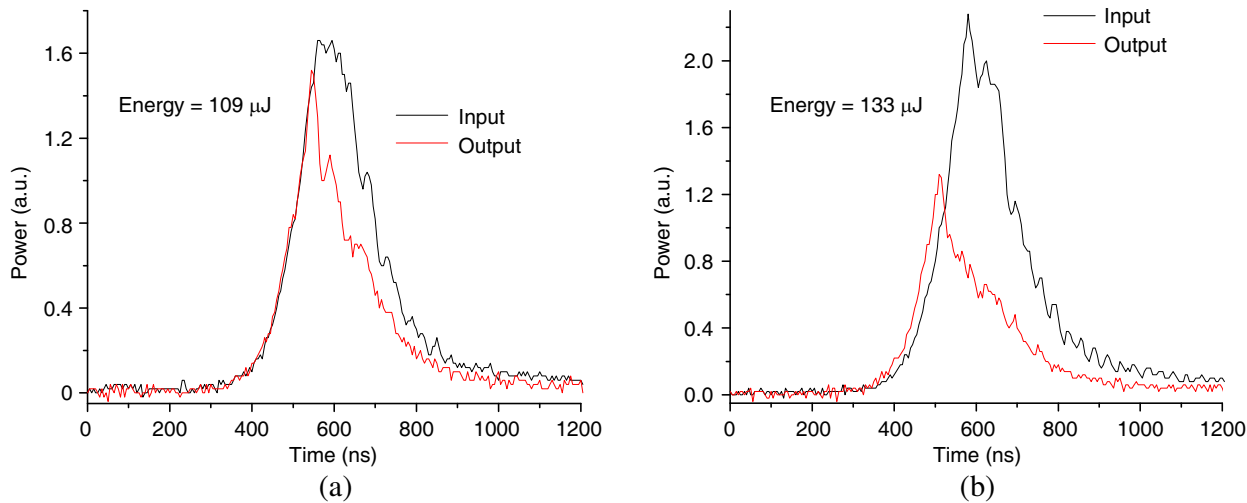

Figure 5. (a) Oscilloscope traces of the input and output laser pulses for input laser energy = 109 μJ; (b) input laser energy = 133 μJ. Pulse duration 300 ns; laser beam spot diameter: 140 μm.

3. INTENSE LASER INDUCED LATTICE DISTORTION IN BPLC WITH NANOSECONDS AND PICOSECONDS LASERS

Recent studies have shown that another mesophase, namely, Blue-Phase Liquid Crystals (BPLC) present promising *alternatives to NLC* for electro- and nonlinear optics [32–44]. In this unique class of optical materials formed by mixing a chiral compound and nematics, the molecules self-assemble (without cell-surface alignment) into tightly wound defect-spirals that form 3-D body-centered cubic or simple cubic lattices with *sub-wavelength* lattice constants, cf. Figure 7. These blue-phase liquid crystals are therefore *optically isotropic.* Optical properties such as refractive index and responses of BPLC are generally independent of the laser polarization and direction of incidence, unlike birefringent NLC; yet their optical nonlinearities have been shown to be of comparable magnitude to those of nematics.

Following the general discussion in previous sections, Maxwell Stress by the optical electric field of intense laser pulses will cause flows in transparent BPLC as well. Out studies [39, 43] have
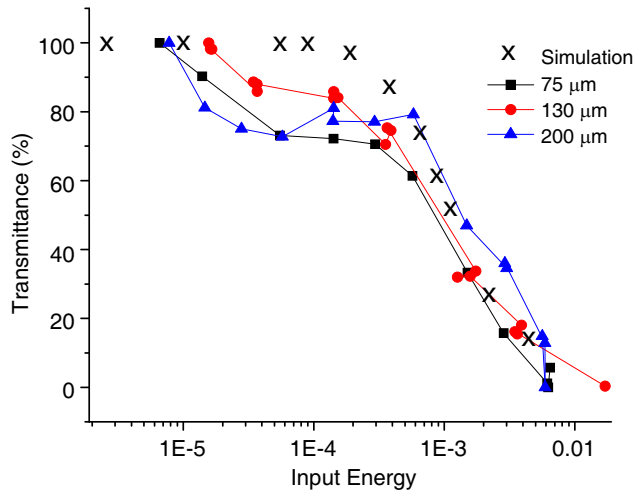
Figure 6. Plot of the dependence of the transmission (*transmitted laser energy vs. the input*) on input laser energy for three NLC sample thicknesses.
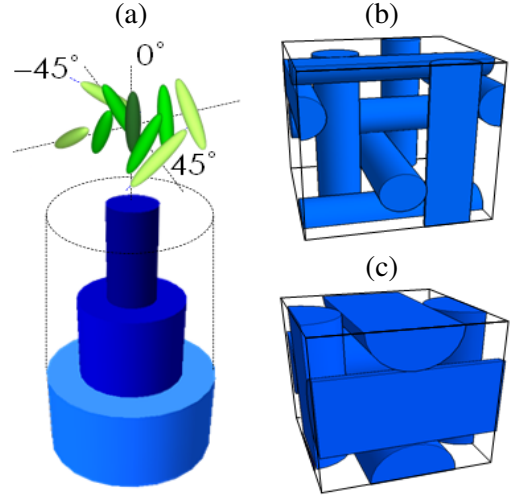

Figure 7. BPLC molecular arrangement and crystalline lattice, (a) molecules in tightly wound double-twist 'cylinder'; (b) BPI phase-body centered cubic lattice; (c) BPII phase-simple cubic lattice.

shown that in general, focused pulsed laser of intensity over several MW/cm^2 is required to generate observable effects. In the case of a Gaussian laser beam with a radial intensity distribution of the form $I(r) \sim |E(t)E^*(t)| e^{-2\frac{r^2}{\omega^2}}$, the Maxwell stress from Equation (1) becomes:

$$\langle f_E \rangle = \varepsilon_0 \varepsilon_\perp |E(t)E^*(t)| e^{-2\frac{x^2+y^2}{\omega^2}} \left[-\frac{x}{\omega^2}, \frac{y}{\omega^2}, 0 \right] \tag{20}$$

The equations describing the resulting flow process thus become:

$$\rho \frac{\partial v_x}{\partial t} - \eta \nabla^2 v_x = f_{E,x} = -\varepsilon_0 \varepsilon_\perp |E(t)E^*(t)| e^{-2\frac{x^2+y^2}{\omega^2}} \cdot \frac{x}{\omega^2} \tag{21a}$$

$$\rho \frac{\partial v_y}{\partial t} - \eta \nabla^2 v_y = f_{E,y} = \varepsilon_0 \varepsilon_\perp |E(t)E^*(t)| e^{-2\frac{x^2+y^2}{\omega^2}} \cdot \frac{y}{\omega^2} \tag{21b}$$

The magnitude of the Maxwell stress is plotted in Figure 8, which depicts a *volcano-shaped* radial dependence with a peak at a radial distance of $\sim 0.7\omega$, and a minimum at the center. Because of
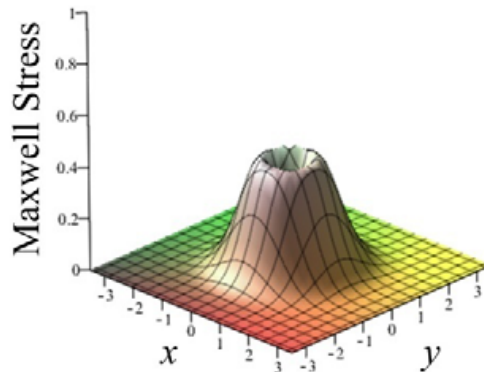

Figure 8. Plot of the radial dependence of the magnitude of the Maxwell stress associated with a Gaussian laser beam.

such radial dependence, flows will take place in all radial directions. A quantitative calculation of the Maxwell Stress induced flow and lattice distortion in BPLC, taking into account the 3-dimensional and time dependent flows and the resulting BPLC lattice distortion and director axis reorientation is rather complex and is outside the scope of this article. However, it is clear from the analysis and results in the preceding section that such radially varying Stress would create a corresponding radially varying lattice distortion and refractive index modulation. Consequently the transmitted laser beam would acquire a transverse phase modulation that results in beam focusing/defocusing and other distortion effects [2, 39, 43, 45–50].

These phase modulation effects have been observed before [43] using nanosecond laser pulses and an experimental set-up shown in Figure 9(a). In the case of a BPLC cell in which the laser induces a negative refractive index change [43], such phase modulation gives rise to a defocused beam with greatly attenuated on-axis power, cf. Figure 9(b). More recently, we have repeated the experiments with a picosecond pulse train [kilohertz repetition rate; individual pulse duration: 2 ps; pulse energy: 200 µJ; $\lambda = 800$ nm; focused laser diameter: ~ 200 µm]. A shutter is used to chop out pulse train of 10 ms duration that acts as the pump beam while a CW low-power 532 nm laser is used to probe the refractive index profile. Similar to previous studies [39, 43], the on axis probe beam power is observed to exhibit a fast/sharp drop to almost vanishing value, cf. photo of transmitted probe beam in Figure 9(a), and recover in fraction of a second after the pump beam is over. The long relaxation time is typical of flows and director axis reorientation, although the exact underlying mechanisms(s) caused by such high intensity ($> \mathrm{GW/cm}^2$) remain to be quantitatively ascertained in ongoing work.

We emphasize again here that Maxwell Stress *is only one of several nonlinear effects* that could be generated by such intense pulsed lasers in transparent liquid crystals. As in most organic materials, although they are transparent in terms of single-photon transitions, the constituent molecules of BPLC do undergo two- or multi-photon absorptions due to the high intensities of the laser [6–12]. Non-radiative processes following photo-absorptions invariably result in significant thermal heating and deformation of the BPLC lattice to create large refractive index changes [35, 39] These thermal effects are clearly in play in our experiment; we have observed that upon longer exposure to the picosecond pulse trains, the transmitted beams all exhibit severe thermal blooming appearance in the transmitted beam, often culminating in the creation of visible bubbles in the liquid crystals. Clearly, more quantitative
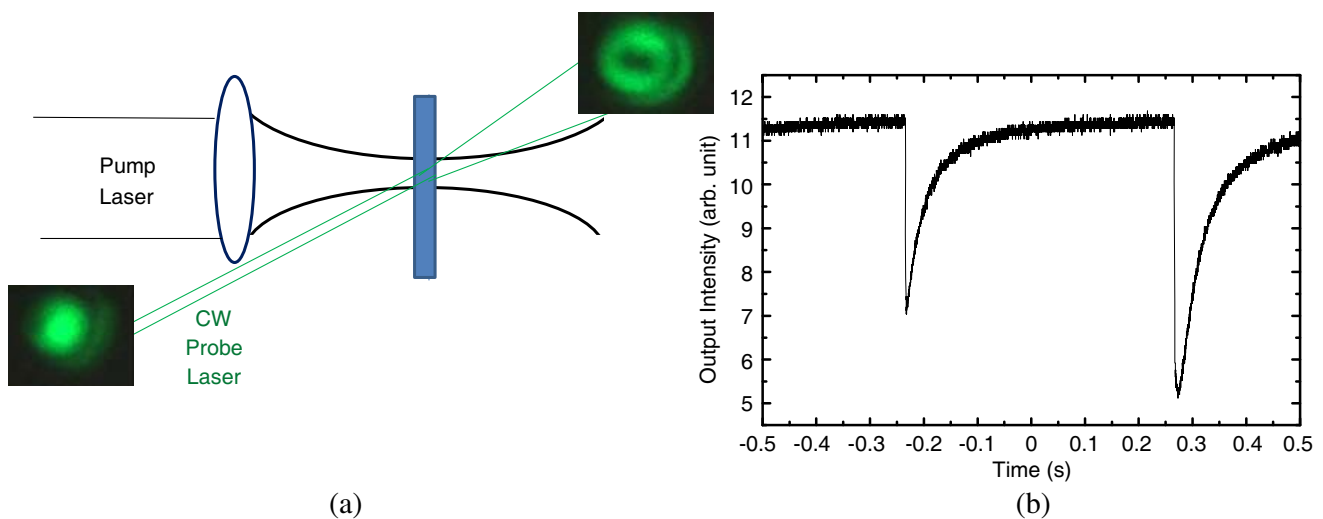

(a)   (b)

Figure 9. (a) Schematic depiction of the experimental set up for probing pulsed laser induced flow and crystalline lattice distortion in BPLC with a CW probe laser; photo inserts show the probe laser beam intensity profiles in the recent picosecond pulse train experiments. (b) Recorded on-axis power of the transmitted probe beam showing an 'instantaneous' drop followed by a slow recovery of the defocusing effect caused by successive nanosecond laser pulses (Pulse duration: 8 ns; pulse energy: 0.02 mJ; laser spot diameter: ~ 150 µm; laser intensity: $\sim 8.3 \mathrm{MW/cm}^2$).
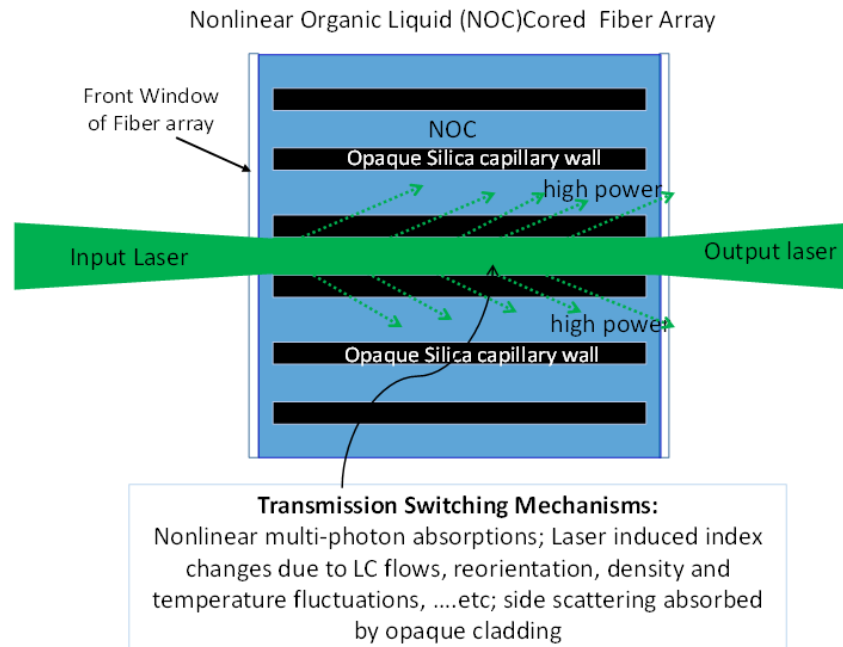
Figure 10. Schematic depiction of the various mechanisms that could come into play in affecting the transmission of a laser pulse through a BPLC cored constituent fiber in a BPLC fiber array for passive sensor protection applications.

experimental and theoretical studies similar to those conducted on NLC are needed, and are currently underway in order to elucidate and quantify the dynamical roles played by Maxwell stress, multi-photon absorptions, heating, electrostriction and other possible index changing mechanisms in BPLC.

For some applications such as optical limiter for passive sensor protection [9–11, 51–54], it is actually an advantage that several mechanisms (besides Maxwell stress) can act in concert to affect the transmission of an intense laser pulse. An example is the nonlinear fiber imaging faceplate depicted in Figure 10 [9–11], which if placed within an optical imaging system will fully transmits low level light from the viewed scenery, but causes high intensity unwanted light (lasers, welder's torch, direct sun light, ...etc.) to self-attenuate efficiently due to these nonlinear optical mechanisms.

4. CONCLUSION

In this article devoted to a special issue commemorating 150 years of Maxwell equations, we have singled out Maxwell Stress induced flow-reorientation effect in transparent liquid crystals as a mechanism to produce laser intensity-dependent refractive index changes, and discuss some aspects of the resulting nonlinear phase modulation and propagation processes. Theoretical simulations and experimental studies have demonstrated that it is a viable mechanism for all-optical switching operations with response times in the sub-microseconds to nanoseconds regime. Since the process is largely independent of the laser frequency or material resonances, it applies to agile frequency laser over the entire visible to near infrared spectral region, albeit with much higher switching thresholds compared to other photo-absorption based mechanisms in liquid crystals.

ACKNOWLEDGMENT

REFERENCES

1. Jackson, J. D., *Classical Electrodynamics*, Wiley, New York, 1975.
2. Khoo, I. C., "Nonlinear optics of liquid crystalline materials," *Physics Report*, Vol. 471, 221–267, 2009.
3. Khoo, I. C., *Liquid Crystals*, 2nd Edition, Wiley, 2007.
4. Christodoulides, D. N., I. C. Khoo, G. J. Salamo, G. I. Stegeman, and E. W. van Stryland, "Nonlinear refraction and absorption: Mechanisms and magnitudes," *Adv. Opt. Photon.*, Vol. 2, 60–200, 2010.
5. Khoo, I. C., "Nonlinear optics, active plasmonic and tunable metamaterials with liquid crystals," *Progress in Quantum Electronics*, Vol. 38, No. 2, 77–117, 2014.
6. Khoo, I. C. and S. Zhao, "Multiple time scales optical nonlinearities of liquid crystals for optical-terahertz-microwave applications," *Progress In Electromagnetic Research*, Vol. 147, 37–56, 2014.
7. He, G. S., L.-S. Tan, Q. Zheng, and P. N. Prasad, "Multi-photon absorbing materials: Molecular designs, syntheses, characterizations, and applications," *Chemical Reviews*, Vol. 108, No. 4, 1245–1330, 2008.
8. Khoo, I. C., S. Webster, S. Kubo, W. J. Youngblood, J. Liou, A. Diaz, T. E. Mallouk, P. Lin, D. Peceli, L. A. Padilha, D. J. Hagan, and E. W. van Stryland, "Synthesis and characterization of the multi-photon absorption and excited-state properties of 4-propyl 4'-butyl diphenyl acetylene," *J. Mater. Chem.*, Vol. 19, 7525–7531, 2009.
9. Khoo, I. C. and A. Diaz, "Multiple-time-scales dynamical studies of nonlinear transmission of pulsed lasers in a multi-photon absorbing organic material," *J. Opt. Soc. Am. B*, Vol. 28, 1702–1710, 2011.
10. Khoo, I. C., A. Diaz, and J. Ding, "Nonlinear-absorbing fiber array for large dynamic range optical limiting application against intense short laser pulses," *J. Opt. Soc. Am. B*, Vol. 21, 1234–1240, 2004.
11. Khoo, I. C., "Nonlinear organic liquid cored fiber array for all-optical switching and sensor protection against short pulsed lasers," *IEEE J. Selected Topics in Quantum Electronics JSTQE*, Vol. 14, No. 3, 946–951, 2008.
12. Song, L., S. Fu, Y. Liu, J. Zhou, V. G. Chigrinov, and I. C. Khoo, "Direct femtosecond pulse compression with miniature-sized Bragg cholesteric liquid crystal," *Optics Letts.*, Vol. 38, 5040–5042, 2013.
13. Khoo, I. C. and R. Normandin, "The mechanism and dynamics of transient thermal grating diffraction in nematic liquid crystal films," *IEEE J. Quant. Electronics*, Vol. 21, 329–335, 1985.
14. Eichler, H. J. and R. Macdonald, "Flow-alignment and inertial effects in picosecond laser-induced reorientation phenomena of nematic liquid crystals," *Phys. Rev. Letts.*, 2666–2669, 1991.
15. Khoo, I. C., R. G. Lindquist, R. R. Michael, R. J. Mansfield, and P. Lopresti, "Dynamics of picosecond laser induced density, temperature and flow-reorientation effects in the mesophases of liquid crystals," *J. Appl. Phys.*, Vol. 69, 3853–3859, 1991.
16. Khoo, I. C., "Laser induced thermal, orientational and density nonlinear optical effects in nematic liquid crystal," *Phys. Rev. A*, Vol. 42, 1001–1004, Jul. 1990.
17. Simoni, F. and O. Francescangeli, "Effects of light on molecular orientation of liquid crystals," *J. Phys.-Cond. Mat.*, Vol. 11, R439–R487, 1999.
18. Blinov, L. M., "Photoinduced molecular reorientation in polymers, Langmuir-Blodgett films and liquid crystals," *JNOPM*, Vol. 5, 165–187, 1996.
19. Li, H., Y. Liang, and I. C. Khoo, "Transient laser induced orthogonal director axis reorientation in dye-doped liquid crystal," *Mol. Cryst. Liq. Cryst.*, Vol. 251, 85–92, 1994.
20. Khoo, I. C., "Re-examination of the theory and experimental results of optically induced molecular reorientation and nonlinear diffractions in nematic liquid crystals: Spatial frequency and temperature dependence," *Phys. Rev. A*, Vol. 27, 2747–2750, 1983.
21. Tabiryan, N. V., A. V. Sukhov, and B. Y. Zeldovich, "Orientatioanl optical nonlinearity of liquid crystals," *Mol. Cryst. Liq. Cryst.*, Vol. 136, 1–139, 1986.

22. Khoo, I. C., "Optical-dc-field induced space charge fields and photorefractive-like holographic grating formation in Nematic liquid crystals," *Mol. Cryst. Liq. Cryst.*, Vol. 282, 53–66, 1996.

23. Yu, H. F. and T. Ikeda, "Photocontrollable liquid-crystalline actuators," *Adv. Mat.*, Vol. 23, 2149–2180, 2011.

24. Ptasinski, J., S. W. Kim, L. Pang, I.-C. Khoo, and Y. Fainman, "Optical tuning of silicon photonic structures with nematic liquid crystal claddings," *Optics Letts.*, Vol. 38, No. 12, 2008–2010, 2013.

25. Liu, Y. J., Q. Hao, J. S. T. Smalley, J. Liou, I. C. Khoo, and T. J. Huang, "A frequency-addressed plasmonic switch based on dual-frequency liquid crystal," *Appl. Phys. Lett.*, Vol. 97, No. 9, article #: 091101, 2010.

26. Xiao, S., U. K. Chettiar, A. V. Kildishev, V. Drachev, I. C. Khoo, and V. M. Shalaev, "Tunable magnetic response of metamaterials," *Appl. Phys. Lett.*, Vol. 95, No. 3, Article Number: 033115, 2009.

27. Graugnard, E., J. S. King, S. Jain, C. J. Summers, Y. Zhang-Williams, and I. C. Khoo, "Electric field tuning of the Bragg peak in large-pore TiO_2 inverse shell opals," *Phys. Rev. B*, Vol. 72, 233105, 2005.

28. Minovich, A., J. Farnell, D. N. Neshev, I. McKerracher, F. Karouta, J. Tian, D. A. Powell, I. V. Shadrivov, H. H. Tan, C. Jagadish, and Y. S. Kivshar, "Liquid crystal based nonlinear fishnet metamaterials," *Appl. Phys. Lett.*, Vol. 100, Article Number: 121113, 2012.

29. Khoo, I. C., J. H. Park, and J. D. Liou, "Theory and experimental studies of all-optical transmission switching in a twist-alignment Dye-doped nematic liquid crystal," *J. Opt. Soc. Am. B*, Vol. 25, 1931–1937, 2008.

30. Khoo, I. C., J. Liou, and M. V. Stinger, "Microseconds-nanoseconds all-optical switching of visible-near infrared ($0.5\,\mu$m–$1.55\,\mu$m) lasers with Dye-doped nematic liquid crystals," *Mole. Cryst. Liq. Cryst.*, Vol. 527, 109–118, 2010.

31. Khoo, I. C., J. Liou, M. V. Stinger, and S. Zhao, "Ultrafast all-optical switching with transparent and absorptive nematic liquid crystals-implications in tunable metamaterials," *Mol. Cryst. Liq. Cryst.*, Vol. 543, 151–159, 2011.

32. Khoo, I. C., "Extreme nonlinear optics of nematic liquid crystals," *J. Opt. Soc. Am. B*, Vol. 28, A45–A55, 2011, Invited paper in Focus Issue dedicated to 50th Anniversary of Nonlinear Optics.

33. Coles, H. J. and M. N. Pivnenko, "Liquid crystal 'blue phases' with a wide temperature range," *Nature*, Vol. 436, 997–1000, 2005.

34. Tiribocchi, A., G. Gonnella, D. Marenduzzo, and E. Orlandini, "Switching dynamics in cholesteric blue phases," *Soft Matter*, Vol. 7, 3295–3306, 2011.

35. Chen, C. W., H. C. Jau, C. H. Lee, C. C. Li, C. T. Hou, C. W. Wu, T. H. Lin, and I. C. Khoo, "Temperature dependence of refractive index in blue phase liquid crystals," *Optical Materials Express*, Vol. 3, No. 5, 527–532, 2013.

36. Khoo, I. C. and T. H. Lin, "Nonlinear optical grating diffraction in dye-doped blue-phase liquid crystals," *Optics Letts.*, Vol. 37, 3225–3227, 2012.

37. Lin, T.-H., Y. Li, C.-T. Wang, H.-C. Jau, C.-W. Chen, C.-C. Li, H. K. Bisoyi, T. J. Bunning, and Q. Li, "Red, green and blue reflections enabled in an optically tunable self-organized 3D cubic nanostructured thin film," *Advanced Materials*, Vol. 25, No. 36, 5050-4, 2013.

38. Chen, C.-W., H.-C. Jau, C.-T. Wang, C.-H. Lee, I. C. Khoo, and T.-H. Lin, "Random lasing in blue phase liquid crystals," *Optics Express*, Vol. 20, No. 21, 23978–23984, 2012.

39. Khoo, I. C., K. L. Hong, S. Zhao, D. Ma, and T.-H. Lin, "Blue-phase liquid crystal cored optical fiber array with photonic bandgaps and nonlinear transmission properties," *Optics Express*, Vol. 21, No. 4, 4319–4327, 2013.

40. Ptasinski, J., I.-C. Khoo, and Y. Fainman, "Enhanced optical tuning of modified-geometry resonators clad in blue phase liquid crystals," *Optics Letts.*, Vol. 39, 5435–5438, 2014.

41. Khoo, I. C., "Dc-field assisted grating formation and nonlinear diffraction in Methyl-red Dye-doped blue-phase liquid crystals," *Optics Letts.*, Vol. 40, 60–63, 2015.

42. Ptasinski, J., I.-C. Khoo, and Y. Fainman, "Enhanced optical tuning of modified-geometry resonators clad in blue phase liquid crystals," *Optics Letts.*, Vol. 39, 5435–5438, 2014.

43. Khoo, I. C., C. W. Chen, K. L. Hong, T. H. Lin, and S. Zhao, "Nonlinear optics of nematic and blue phase liquid crystals," *Molecular Crystals Liquid Crystals*, Vol. 594, No. 1, 31–41, 2014.

44. Chen, C.-W., T.-H. Lin, and I. C. Khoo, "Dynamical studies of the mechanisms for optical nonlinearities of methyl-red Dye doped blue phase liquid crystals," *Optics Express*, Vol. 23, 21650–21656, 2015.

45. Khoo, I. C., P. Y. Yan, T. H. Liu, S. Shepard, and J. Y. Hou, 'Theory and experiment on optical transverse intensity bistability in the transmission through nonlinear thin (nematic liquid crystal) film," *Phys. Rev. A*, Vol. 29, 2756–2764, 1984.

46. Khoo, I. C., J. Y. Hou, T. H. Liu, P. Y. Yan, R. R. Michael, and G. M. Finn, "Transverse self-phase modulation and bistability in the transmission of a laser beam through a nonlinear thin film," *J. Opt. Soc. Am. B*, Vol. 4, 886–891, 1987.

47. Bloisi, F., L. Vicari, F. Simoni, G. Cipparrone, and C. Umeton, "Self-phase modulation in nematic liquid crystls films — Detailed measurements and theoretical calculations," *J. Opt. Soc. Am. B*, Vol. 5, 2462–2466, 1988.

48. Khoo, I. C., P. Y. Yan, and T. H. Liu, "Nonlocal radial dependence of laser-induced molecular reorientation in a nematic liquid crystal film — Theory and experiment," *J. Opt. Soc. Am. B*, Vol. 4, 115–120, 1987.

49. Wu, J. J., S. H. Chen, J. Y. Fan, and G. S. Ong, "Propagation of a Gaussian-profile laser beam in nematic liquid crystals and the structure of its nonlinear diffraction rings," *J. Opt. Soc. Am. B*, Vol. 7, 1147–1157, 1990.

50. Peccianti, M. and G. Assanto, "Nematicons," *Phys. Report*, Vol. 516, 147–208, 2012.

51. Khoo, I. C., G. Finn, R. R. Michael, and T. H. Liu, "Passive optical self-limiter using laser induced axially symmetric and asymmetric transverse self-phase modulations in a liquid crystal film," *Optics Letts.*, Vol. 11, 227–229, 1986.

52. Justus, B. L., A. L. Huston, and A. J. Campillo, "Broad-band thermal optical limiter," *Appl. Phys. Lett.*, Vol. 63, 1483–1485, 1993.

53. Khoo, I. C. and H. Li, "Nonlinear optical propagation and self-limiting effect in liquid crystalline fiber," *Appl. Phys. B*, Vol. 59, 573–580, 1994.

54. Hernandez, F. E., S. S. Yang, V. Dubikovskty, W. Shensky, E. W. van Stryland, and D. J. Hagan, "Dual focal plane visible optical limiter," *JNOPM*, Vol. 9, 423–440, 2000.